The Constrained-Network Propagation (C-NetP) Technique to Improve SBAS-DInSAR Deformation Time Series Retrieval

Chandrakanta Ojha, Michele Manunta, Riccardo Lanari, *Fellow, IEEE*, and Antonio Pepe, *Member, IEEE*

***Abstract*—We present an innovative region-growing-based technique that permits to improve the surface displacement time-series retrieval capability of the two-scale Small BAseline Subset (SBAS) Differential Interferometric Synthetic Aperture Radar (DInSAR) approach in medium-to-low coherence regions. Starting from a sequence of multitemporal differential SAR interferograms, computed at the full spatial resolution scale, the developed method "propagates" the information on the deformation relevant to a set of high coherent SAR pixels [referred to as source pixels (SPs)], in correspondence to which SBAS-DInSAR deformation measurements have previously been estimated, to their less coherent neighbouring ones. In this framework, a minimum-norm constrained optimization problem, relying on the use of constrained Delaunay triangulations (CDTs), is solved, where the constraints represent the displacement values at the SP locations. Such DInSAR processing scheme, referred to as Constrained-Network Propagation (C-NetP), is easy to implement and, although specifically developed to work within the two-scale SBAS framework, it can be extended to wider DInSAR scenarios. The validity of the method has been investigated by processing a SAR dataset acquired over the city of Rome (Italy) by the Cosmo-SkyMed constellation from July 2010 to October 2012. The achieved results demonstrate that the proposed C-NetP method is capable to significantly increase the spatial density of the SBAS-DInSAR measurements, reaching an improvement of about 250%. Such an improvement allows revealing deformation patterns that are partially or completely hidden, by applying the conventional two-scale SBAS processing. This is particularly relevant in urban areas where the assessment and management of the risk associated to the deformation affecting infrastructures is strategic for decision makers and local authorities.**

***Index Terms*—Constrained optimization problems, deformation, Delaunay triangulations, Differential Interferometric Synthetic Aperture Radar (DInSAR), Small BAseline Subset (SBAS), time series.**

Manuscript received March 16, 2015; revised July 09, 2015; accepted September 16, 2015. Date of publication October 29, 2015; date of current version January 08, 2016. This work was supported in part by the Italian Space Agency (ASI), in part by Italian Department of Civil Protection (DPC), and in part by the Italian Ministero dell'Istruzione, dell'Università e della Ricerca (MIUR) under the project entitled "Studio multidisciplinare della fase preparatoria di un terremoto.' Part of the this research has been carried out through the I-AMICA (Infrastructure of High Technology for Environmental and Climate Monitoring-PONa3_00363) project of Structural improvement financed under the National Operational Programme (PON) for "Research and Competitiveness 2007–2013," co-funded with European Regional Development Fund (ERDF) and National resources.

The authors are with the Istituto per il Rilevamento Elettromagnetico dell'Ambiente (IREA), National Council of Research (CNR), Naples 328 NA, Italy (e-mail: ojha.c@irea.cnr.it; manunta.m@irea.cnr.it; pepe.a@irea.cnr.it; lanari.r@irea.cnr.it).

Color versions of one or more of the figures in this paper are available online at http://ieeexplore.ieee.org.

Digital Object Identifier 10.1109/JSTARS.2015.2482358

I. Introduction

DIFFERENTIAL synthetic aperture radar interferometry (DInSAR) [1], [2] is nowadays a well-consolidated technique for the monitoring of Earth's surface deformations. Traditionally developed to investigate single deformation episodes [3]–[7], the DInSAR methodology has afterward been extended to investigate the temporal evolution of the surface displacements through the development of the so-called "advanced" multitemporal DInSAR approaches [8]–[16], implementing proper inversions of sequences of SAR interferograms computed between pairs of SAR data collected at different time epochs. Over almost the past 15 years, several advanced DInSAR methodologies have been presented; they can be broadly grouped in the two main categories of the Persistent Scatterer (PS) [8]–[11] and the Small Baseline (SB) [12]–[16] approaches. While PS techniques are mostly focused on analyzing point-like targets that are not significantly affected by decorrelation effects [17], [18], the SB methods allow the investigation of deformation signals related to distributed scatterers (DS) on the ground, which can be instead severely corrupted by decorrelation effects. In this latter case, an *a priori* selection of the exploited SAR data pairs with SB[1] values is required to reduce the noise levels in the generated interferograms [17]. Despite of their intrinsic differences, both the PS and SB algorithms have successfully been used to detect and monitor deformation phenomena due to several natural and anthropic hazards, such as volcanic events, earthquakes, landslides, damages to man-made infrastructures in urbanized areas caused by underground, and tunneling excavations and/or gas and water exploitation [19]–[29]. Nevertheless, the existing advanced multitemporal DInSAR approaches exhibit some specific limitations affecting their own performances. In particular, one limiting factor of the SB techniques resides in their reduced capability to correctly investigate deformation signals associated with isolated targets that are fully (or partly) embedded in regions on the ground characterized by low spatial coherence values, as well as in their difficulties to correctly analyze displacement signals with very high rates both in space and time. In such cases, the correct identification of coherent targets' location and the subsequent analysis of their relevant deformation signals are rather critical, especially while working at the full spatial resolution scale (i.e., at the scale of

[1]The baseline represents the spatial/temporal separation between the acquisition orbits of the investigated SAR data pair.

single-look interferograms), making the risk to incur in "false alarm" conditions more likely.

To mitigate these problems, we present in this paper an innovative DInSAR processing scheme, which relies on the application of a network-optimization strategy. This solution is able to improve the performance of the well-known two-scale Small BAseline Subset (SBAS) technique [13] for the retrieval of deformation time series at the full-resolution spatial scale. The basic idea is to take profit from the previously retrieved deformation (and residual topography) estimates relevant to a group of highly coherent targets, and simply "to propagate" this information to less coherent neighboring regions. To achieve this task, we have properly extended to a wider scenario the constrained optimization strategy originally proposed in [30] for the analysis of PS targets displacement through the Extended Minimum Cost Flow (EMCF) phase unwrapping (PhU) algorithm [31]. More specifically, the proposed DInSAR optimization scheme, hereinafter referred to as Constrained-Network Propagation (C-NetP), starts from the computation of deformation values in correspondence to a group of very coherent pixels on the ground, referred to as "source pixels" (SPs). In particular, the SP displacement time series, which remain unchanged after the processing operation, is obtained as the result of a preliminary processing step performed by using the (conventional) two-scale SBAS processing algorithm [13]. Accordingly, SPs are successfully identified by calculating, for each investigated target on the ground, the inherent value of the temporal coherence factor [13]. The "propagation" of the solution from such very coherent targets to their neighboring ones allows us to drastically increase the coherent pixel density of the SBAS-DInSAR results. Indeed, critical points with moderate-to-low temporal coherence values can be initially discarded (imposing larger temporal coherence thresholds) and, only subsequently, recovered via the proposed C-NetP strategy, thus appreciably reducing the probability to incur in "false alarm" conditions.

The proposed method has been validated through a series of experiments carried out on a sequence of differential SAR interferograms computed at the full spatial resolution scale over the city of Rome (Italy) using an archive of SAR data collected by the COSMO-SkyMed (CSK) sensor constellation [32]. The achieved results demonstrated the effectiveness of the proposed strategy, proving its capability to increase the density of DInSAR measurements.

This paper is organized as follows. Section II provides the general formulation of the constrained network optimization problem, which is at the base of the C-NetP approach. The rationale of the method as well its practical implementation is described in Section III. Experimental results are presented in Section IV, whereas conclusions and further developments are addressed in Section V.

II. Constrained Network Optimization Problem

This section introduces the theoretical framework at the base of the proposed DInSAR C-NetP processing scheme (which is fully detailed in Section III), relying on the solution of a constrained optimization problem [33] for the PhU operation of differential SAR interferograms.

A. Formulation of the L_p PhU Problem

To introduce the problem at hand, let us first refer to one single differential SAR interferogram, and let ϕ and ψ be the wrapped (measured) and unwrapped (unknown) interferometric phases, respectively. PhU operation [34]–[43] basically consists in searching for the (unknown) 2π-integer multiples, namely K, that have to be added to the wrapped phase to determine the unwrapped (full) interferometric phase at the same grid locations, that is:

$$\phi(P) = \psi(P) + 2\pi K(P) \quad \forall P \in V \tag{1}$$

where V is a discrete (and generally irregular) grid of coherent SAR pixels of the azimuth/range $A_Z \times R_G$ spatial domain. On irregular grids, PhU is usually performed by first computing a planar connected graph $\mathbf{G} = \{\mathbf{V}, \mathbf{E}\}$ (e.g., a Delaunay triangulation [44]), where $\mathbf{V}$ is the set of vertexes and $\mathbf{E}$ is the corresponding set of N_E edges. The wrapped (measured) phase difference $\Delta\phi_q = \Delta\phi_{AB} = Wr[\phi(A) - \phi(B)]$, calculated over the generic qth edge of the graph $\mathbf{G}$ that connects the points A and B of the spatial domain [see for instance the arc highlighted in Fig. 1(a)], can be then related to the corresponding (unknown) unwrapped phase difference $\Delta\psi_q = \Delta\psi_{AB} = \psi(A) - \psi(B)$, as follows:

$$\Delta\psi_q = \Delta\psi_{AB} = \psi(A) - \psi(B) = \Delta\phi_q + 2\pi H_q \tag{2}$$

where in $H_q = [K(A) - K(B)] + [\phi(A) - \phi(B) - \Delta\phi_q]/2\pi$, and $Wr(\cdot)$ is the wrapping operator that wraps all values of its argument into the $(-\pi, \pi)$ range by adding (or subtracting) an integral number of 2π rad from its argument. Given the wrapped phase values $\{\Delta\phi_q\}_{q=1}^{N_E}$ and a corresponding set of (properly chosen) weighting costs $\{w_q\}_{q=1}^{N_E}$, which are mapped over the arcs of the network graph $\mathbf{G}$, the most general formulation of a (weighted) minimum L_{p} norm PhU problem consists in the solution of the following nonlinear optimization [35]:

$$\psi = \text{argmin}\left[\sum_{q=1}^{N_E-1} w_q |\Delta\psi_q - \Delta\phi_q|^p\right] \tag{3}$$

The problem stated in (3) is a global minimization since all the observed phases are needed to compute the unwrapped phase in a given pixel, and its complexity is strictly dependent on the connectivity characteristics of the exploited graph $\mathbf{G}$. With $p = 2$, the problem in (3) becomes a least-squares optimization problem that has analytical solutions [36]. However, a drawback of the L_2 norm is that it tends to smooth discontinuities, not preserving the 2π difference constraint between unwrapped and wrapped phases (i.e., it is not ensured that the terms K in (1) assume integer values). For the above-mentioned reasons, L_1 norm is usually preferred to the L_2 one; in this case, the problem in (3) can be equivalently stated [see (2)] as follows:

$$\begin{aligned}\mathbf{H} &= \text{argmin}\left[\sum_{q=1}^{N_E-1} w_q \left|\Delta\psi_q - \Delta\phi_q\right|\right] \\ &= \text{argmin}\left[2\pi \sum_{q=1}^{N_E-1} w_q \left|H_q\right|\right]\end{aligned} \tag{4a}$$

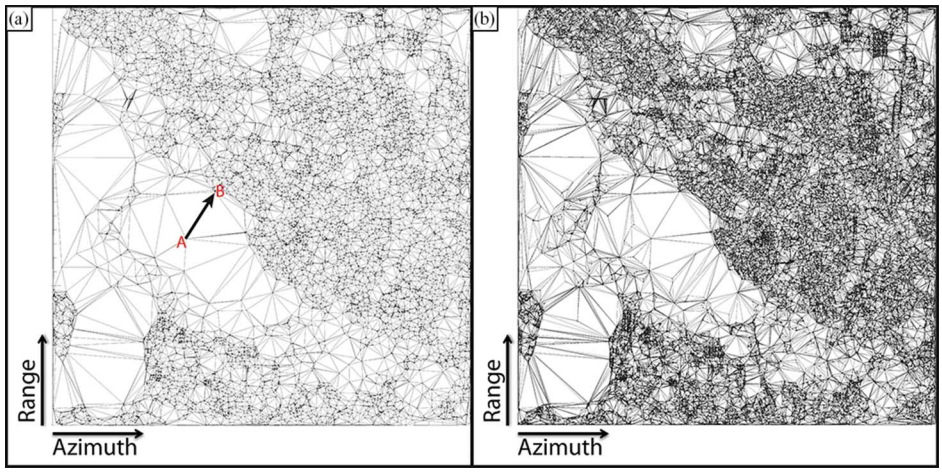

Fig. 1. Spatial network in the azimuth/range spatial domain involving a set of spatially coherent pixels. (a) Delaunay triangulation related to very coherent SPs used in the following experiments. (b) CDT relevant to the TPs.

subject to:

$$\sum_{i=1}^{Q} \Delta\psi_i = \sum_{i=1}^{Q} \Delta\phi_i + 2\pi \sum_{i=1}^{Q} H_i = 0 \tag{4b}$$

where condition (4b) ensures that unwrapped phase gradients $\Delta\psi_q, \quad q = 1, \ldots, N_E - 1$, define a spatially irrotational field, with Q being the number of edges of any possible closed loop, namely ℓ, into the graph $\mathbf{G}$. Noteworthy, as said earlier, for practical implementations, the graph $\mathbf{G}$ is formed by elementary loops that consist of triangles [see Fig. 1(a)], and a Delaunay triangulation [44] is typically computed.

The problem in (4a) and (4b) has been solved by Flynn [40] and Costantini [36], [42] by reformulating it in terms of an equivalent minimum cost flow (MCF) network problem, for which efficient network programming codes (i.e., the RELAX IV [45]) are available; the only requirement is that the graph $\mathbf{G}$ is planar and fully connected (see [42] for more details).

B. Formulation of the Constrained L_p PhU Problem

In this subsection, we analyze the more general case [with respect to (4a) and (4b)] that arises for the solution of a constrained PhU problem. In this framework, it is additionally required that unwrapped phases corresponding to a subset of radar pixels, namely $S \subseteq V$, have to be constrained (bounded) to assume specific and *a priori* known values $\psi(P) = \psi'(P) \, \forall P \in S$, which must remain unchanged after PhU processing operation. Eventually, the following constrained (weighted) minimum L_p norm optimization problem has to be solved:

$$\psi = \text{argmin}\left[\sum_{q=1}^{N_E-1} w_q |\Delta\psi_q - \Delta\phi_q|^p\right] \tag{5a}$$

subject to:

$$\psi(P) = \psi'(P) \quad \forall P \in S. \tag{5b}$$

We can easily recognize that the solution of the constrained problem in (5a) and (5b) can be efficiently (and generally) achieved, extending what originally proposed in [30], through the computation of a "primary," connected subgraph $\mathbf{G}' = \{\mathbf{V}', \mathbf{E}'\}$ from the set of bounded pixels S and, subsequently, by considering a "secondary" constrained graph [46] that contains all the edges $\mathbf{E}'$ of the primary network, i.e., $\mathbf{E}' \subseteq \mathbf{E}$. We remark that constrained graphs are largely used in constrained satisfaction [47], [48] and network optimization problems [49], [50] where they are used to solve more complex problems arising from the introduction of additional constraints in canonical linear and/or nonlinear programming problems.

In such a way, over the N'_E edges $\mathbf{E}'$ of $\mathbf{G}'$, the unwrapped phase differences, namely $\{\Delta\psi'_h\}_{h=1}^{N'_E}$, are completely known and, accordingly, the solution of the problem (5a) and (5b) is the same as

$$\psi = \text{argmin}\left[\sum_{q=1}^{N_E-1} \mu_q |\Delta\psi_q - \Delta\Theta_q|^p\right] \tag{6a}$$

with

$$\mu_q = \begin{cases} w_q & e_q \notin \mathbf{E}' \\ L & e_q \in \mathbf{E}', \end{cases} \quad \Delta\Theta_q = \begin{cases} \Delta\phi' & e_q \notin \mathbf{E}' \\ \Delta\psi' & e_q \in \mathbf{E}' \end{cases} \tag{6b}$$

where L (see also [30]) is a very large number which is representative of the infinite value. In this manner, the unwrapped phase differences over the edges of the primal network $\mathbf{G}'$ are fully preserved[2]. It is instructive to note that the problem in (6a) and (6b) is formally identical to the problem in (3), and, in particular, to its particularization to the case of the L_1 norm [see (4a) and (4b)], which is reported in the following for the sake of completeness:

$$\mathbf{H} = \text{argmin}\left[2\pi \sum_{q=1}^{N_E-1} \mu_q |H_q|\right] \tag{7a}$$

[2]As a matter of fact, the problem in (6a) and (6b) is a minimization and, accordingly, any additional correction w.r.t. the phase differences over the edges E' would correspond to an "infinite" (depending on L) cost of the solution, thus no further corrections are automatically guaranteed.

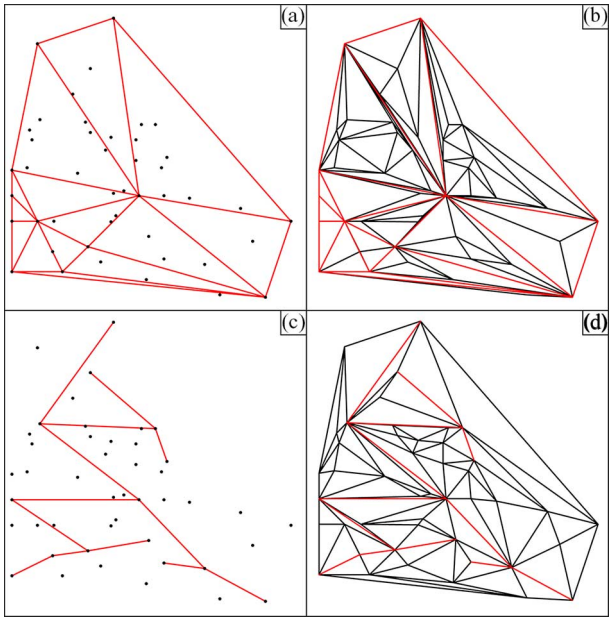

Fig. 2. Examples of CDTs relevant to the discrete set of (black) vertexes drawn in (a)–(d); in (a) and (c) the constrained edges (red arcs) are shown, whereas in (b) and (d) are depicted the corresponding CDTs, where constrained edges are drawn in red and the unconstrained ones in black.

subject to:

$$\sum_{i=1}^{Q} \Delta\phi_i + 2\pi \sum_{i=1}^{Q} H_i = 0 \tag{7b}$$

with

$$\mu_q = \begin{cases} w_q & e_q \notin \mathbf{E}' \\ L & e_q \in \mathbf{E}' \end{cases}, \quad \Delta\Theta_q = \begin{cases} \Delta\phi' & e_q \notin \mathbf{E}' \\ \Delta\psi' & e_q \in \mathbf{E}'. \end{cases} \tag{7c}$$

We remark that the framework represented by the PhU problems in (5a) and (5b), (6a) and (6b), and (7a)–(7c) is extremely wide, including almost all familiar existing PhU approaches. More importantly, such an optimization scheme is large enough to also include recently developed 3-D (e.g., [51], [52]) and mixed space-time PhU approaches [30], [31], [53], only requiring a few adaptations. We remark, in particular, that the approach originally described in [30] represents the particularization of the optimization scheme provided in (7a)–(7c) to the case when EMCF PhU algorithm is used.

For the practical implementation of such a constrained optimization procedure, the generation of the (planar) constrained graph $\mathbf{G}'$ is, hence, required. This is efficiently done by computing a so-called constrained triangulation and, in particular, a constrained delaunay triangulation (CDT). CDTs are used in different fields of technology and science (computer graphic, physics, etc.) [33], [54] and are defined as follows: they are essentially triangulations including a specified set of edges referred to as constraints or constrained edges and are as close as possible to Delaunay triangulations[3]. A few examples of CDTs are shown in Fig. 2, related to a specified set of points and for two different sets of constrained edges. In particular, Fig. 2(a) and (b) represents the case of a set of constrained edges constituting a (connected) spatial redundant network, and Fig. 2(c) and (d) represents the case when they form a spanning tree. In Fig. 1(b), we also show the CDT corresponding to the set of constrained edges of the network depicted in Fig. 1(a) related to the case-study area of the city of Rome used for the experiments presented in Section IV.

[3]Interested readers can find a comprehensive description of CDTs and additional details in [30].

III. C-NetP Algorithm

We extend here the constrained optimization procedures described in Section II to a multitemporal framework, where sequences of differential SAR interferograms need to be jointly managed, showing how these methods can be profitably used for the generation of surface deformation time series through advanced DInSAR analyzes.

The developed constrained-network propagation method, hereinafter referred to as C-NetP, is a two-stage algorithm that, starting from the preliminary knowledge of the deformation time series corresponding to a group of (coherent) points, is capable to drastically improve surface deformation retrieval capability performance by: 1) soundly identifying the set of coherent SAR pixels characterized by deformation signals with suitable levels of accuracy, 2) increasing the number of detectable targets on the ground by "propagating" the "correct" solution from highly coherent radar pixels to nearby regions with reduced level of coherence.

The developed C-NetP DInSAR optimization scheme can also be potentially used with no restrictions at all on the way the preliminary displacement time series are retrieved. For instance, a PS-oriented approach could also be exploited to perform such a preliminary step, while a general purpose SB-oriented approach could be possibly applied to compute the "propagated" displacement time series, following the solution of the constrained optimization problem.

In Section IIIA, we first present the rationale of the C-NetP method, whereas in Section IIIB, we concentrate on the implementation of the constrained PhU optimization procedure within the C-NetP processing framework.

A. Algorithm Rationale

To describe in details the C-NetP algorithm, let us start by considering a set of $\mathrm{N}+1$ SAR scenes collected at the ordered epochs $[t_0, t_1, \ldots t_N]^T$ properly coregistered with respect to a reference (i.e., the master one) scene, namely the one acquired at t_m. A preliminary step is accomplished to retrieve in correspondence to a group of so-called SPs on the ground, namely $\{SP\}$, the relevant deformation time series (corrupted by atmospheric artefacts [8], [12]), namely $\mathbf{d}(P) = [0, d_1(P), d_2(P), \ldots, d_N(P)]^T \quad \forall P \in SP$, where $d_i(P)$ is the deformation at time t_i estimated with respect to the first time acquisition t_0. As said earlier, even though the method has been designed to improve performances of the conventional two-scale SBAS approach [13], the first step of the C-NetP scheme can be either performed using one of currently available DInSAR tools or exploiting displacement measurements inferred from leveling/GPS campaigns (possibly both kind of measurement values could be concurrently available).

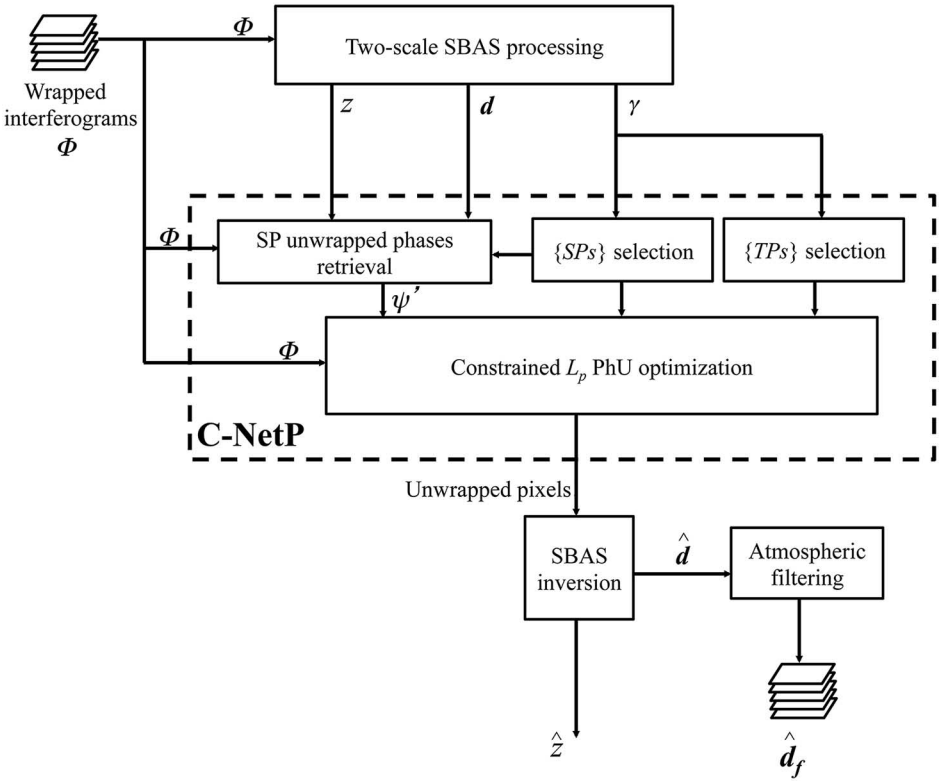

Fig. 3. Block diagram of the proposed C-NetP DInSAR processing scheme.

Furthermore, let us assume to have an estimate of topographic height inaccuracies of the digital elevation model (DEM) used for the generation of the interferograms, namely $z(P) \quad \forall P \in \{SP\}$, as retrieved in correspondence to the SPs' location as an ancillary product of the preliminary step for the generation of DInSAR displacement time series. Generally, the identification of the SPs is done by computing a quality factor on the retrieved displacement time series, namely γ, which is inferred by analyzing the interferometric phase history of the stack of used DInSAR interferograms. As a matter of fact, for the practical implementation of the PS [8], [9] and the SBAS DInSAR processing chains [12], two distinct temporal coherence factors are typically provided, which can be used for the purpose. Eventually, the location of coherent SPs is thus identified as follows:

$$\{SP\} = \{P \in A_Z \times R_G : \gamma(P) \geq \alpha\} \tag{8}$$

where α is a properly chosen threshold.

Once SPs location is identified, the second stage of the C-NetP DInSAR processing scheme consists in solving a constrained (weighted) L_p-norm PhU problem, which is performed on a sequence of M multitemporal differential SAR interferograms, namely $\{\phi_j\}_{j=1}^{M}$. This step relies on the global optimization problem stated in (6), which can be either applied to each SAR interferograms, separately, or concurrently to the stack of interferograms by adjusting the existing conventional 2-D [34]–[38] and 3-D [51], [52] (or mixed hybrid 2-D+2-D space-time [30], [31], [53]) PhU strategies to the newly constrained optimization framework.

B. C-NetP Processing Implementation

The implementation of the proposed C-NetP method requires the preliminary computation of a sequence of unwrapped phases, namely $\{\psi'_j\}_{j=1}^{M}$, in correspondence to the group of high-coherent SPs (previously identified during the first stage of the algorithm), which are subsequently used as constraints into the constrained optimization schemes (6a) and (6b) or (7a)–(7c). As a consequence, on the selected SPs, the unwrapped phases are totally preserved during subsequent constrained optimization procedures. Specifically, the unwrapped phase values corresponding to SPs are calculated as follows:

$$\begin{aligned}\psi'_j(P) = {} & \frac{4\pi}{\lambda}\frac{b_{\perp j}}{r sin\vartheta} z(P) + \frac{4\pi}{\lambda}\left[d_{IM_j}(P) - d_{IS_j}(P)\right] \\ & + Wr\left\{\phi_j(P) - \frac{4\pi}{\lambda}\frac{b_{\perp j}}{r sin\vartheta} z(P) \right. \\ & \left. - \frac{4\pi}{\lambda}\left[d_{IM_j}(P) - d_{IS_j}(P)\right]\right\} \\ & \forall P \in \{SP\} \quad \forall j = 1, \ldots, M\end{aligned} \tag{9}$$

where r is the sensor-to-target distance, λ is the operational wavelength, ϑ is the side-looking angle of the imaged scene, $[IM_1, IM_2, \ldots, IM_M]^T$ and $[IS_1, IS_2, \ldots, IS_M]^T$ are the indexes of the "master" and "slave" time acquisitions related to the selected SAR data pairs[4], whereas $[b_{\perp 1}, b_{\perp 2}, \ldots, b_{\perp M}]^T$

[4]The selection of SAR data pairs, involved in the optimization scheme, depends on the specific DInSAR processing tool used for the optimization. For instance, in a PS-like framework [8], [9], single-master SAR data pairs are selected, whereas in an SB context [12], a set of small baseline multi-master SAR data pairs is considered.

TABLE I
CSK SAR DATASET

Serial no.	Sensor	Acquisitions			Perpendicular baseline (m)
		Day	Month	Year	
1	CSK	04	07	2010	–14.5372
2	CSK	12	07	2010	164.783
3	CSK	21	07	2010	–247.927
4	CSK	28	07	2010	–409.790
5	CSK	05	08	2010	–478.018
6	CSK	13	08	2010	55.2373
7	CSK	07	09	2010	–150.937
8	CSK	22	09	2010	371.832
9	CSK	09	10	2010	0.00000
10	CSK	25	10	2010	–466.347
11	CSK	21	03	2011	476.800
12	CSK	06	04	2011	–39.4341
13	CSK	22	04	2011	–892.674
14	CSK	08	05	2011	–463.743
15	CSK	24	05	2011	–1238.58
16	CSK	09	06	2011	–33.3258
17	CSK	25	06	2011	–696.141
18	CSK	11	07	2011	–815.864
19	CSK	28	08	2011	–842.453
20	CSK	10	09	2011	–872.497
21	CSK	13	09	2011	72.3982
22	CSK	29	09	2011	148.631
23	CSK	15	10	2011	119.730
24	CSK	16	11	2011	–125.073
25	CSK	03	01	2012	–609.794
26	CSK	19	01	2012	–883.403
27	CSK	04	02	2012	–490.917
28	CSK	20	02	2012	230.572
29	CSK	07	03	2012	–756.717
30	CSK	23	03	2012	–1026.44
31	CSK	08	04	2012	–197.475
32	CSK	10	05	2012	–1050.83
33	CSK	15	06	2012	–143.655
34	CSK	23	06	2012	–682.651
35	CSK	09	07	2012	–146.449
36	CSK	25	07	2012	–523.026
37	CSK	10	08	2012	–600.401
38	CSK	26	08	2012	–909.472
39	CSK	11	09	2012	–494.246
40	CSK	01	10	2012	–872.161

is the corresponding vector of interferometric perpendicular baselines. Note that starting from the knowledge of the surface deformation time series at the location of SPs, the relative constrained deformation occurred between the "master" and "slave" time acquisitions for each single SAR data pair is then computed by simply differencing the known displacement time series.

It is worth remarking that the residual topography Z represents one of the outputs of the preliminary step of the algorithm that is needed to recover the deformation values at SPs. However, in case the information on "residual" topography was not available (e.g., when the displacement values are inferred through GPS/leveling campaigns), the unwrapped phases at the SPs can still be computed using (9) by simply setting $z(P) = 0\ \forall P \in \{SP\}$. In the latter case, the deformation time series $\mathbf{d}(P) = [0, d_1(P), d_2(P), \ldots, d_N(P)]^T\ \forall P \in \{SP\}$ (used as constraints in the optimization procedure) do not evidently take account for any additive atmospheric signal; accordingly the phase terms in (9) $Wr\{\phi_j(P) - \frac{4\pi}{\lambda}[d_{IM_j}(P) - d_{IS_j}(P)]\}\ \ \forall P \in \{SP\}\ \ \forall j = 1, \ldots, M$ will

TABLE II
INTERFEROMETRIC SAR DATA PAIRS USED FOR THE PRESENTED EXPERIMENT ON CSK DATA

Serial no.	Interferometric pairs	Perpendicular baseline (m)	Interval (days)
1	04072010CSK_12072010CSK	–179.248	8
2	04072010CSK_21072010CSK	233.296	17
3	04072010CSK_28072010CSK	395.101	24
4	04072010CSK_13082010CSK	–697.583	40
5	04072010CSK_07092010CSK	136.338	65
6	04072010CSK_09102010CSK	–145.018	97
7	04072010CSK_06042011CSK	249.313	276
8	04072010CSK_09062011CSK	186.304	340
9	12072010CSK_13082010CSK	109.503	32
10	12072010CSK_22092010CSK	–207.006	72
11	12072010CSK_29092011CSK	160.852	444
12	12072010CSK_15102011CSK	449.735	460
13	12072010CSK_20022012CSK	–659.086	588
14	21072010CSK_28072010CSK	161.771	7
15	21072010CSK_07092010CSK	–969.504	48
16	21072010CSK_08042012CSK	–505.008	627
17	28072010CSK_05082010CSK	682.158	8
18	28072010CSK_25102010CSK	565.409	89
19	28072010CSK_08052011CSK	53.802	284
20	28072010CSK_08042012CSK	–212.243	620
21	28072010CSK_11092012CSK	842.796	776
22	05082010CSK_25102010CSK	–116.813	81
23	05082010CSK_22042011CSK	414.325	260
24	05082010CSK_08052011CSK	–144.186	276
25	05082010CSK_25062011CSK	217.859	324
26	05082010CSK_03012012CSK	131.469	516
27	05082010CSK_04022012CSK	125.385	548
28	05082010CSK_25072012CSK	447.638	720
29	13082010CSK_09102010CSK	55.261	57
30	13082010CSK_13092011CSK	–172.524	396
31	13082010CSK_15102011CSK	–645.276	428
32	07092010CSK_06042011CSK	–111.386	211
33	07092010CSK_16112011CSK	–257.486	435
34	07092010CSK_08042012CSK	46.448	579
35	07092010CSK_15062012CSK	–734.681	647
36	22092010CSK_21032011CSK	–104.948	180
37	22092010CSK_20022012CSK	141.142	516
38	09102010CSK_09062011CSK	331.311	243
39	09102010CSK_13092011CSK	–725.164	339
40	25102010CSK_08052011CSK	–274.284	195
41	21032011CSK_20022012CSK	246.123	336
42	06042011CSK_09062011CSK	–630.577	64
43	06042011CSK_16112011CSK	856.322	224
44	22042011CSK_24052011CSK	345.315	32
45	22042011CSK_25062011CSK	–196.396	64
46	22042011CSK_11072011CSK	–768.477	80
47	22042011CSK_28082011CSK	–502.422	128
48	22042011CSK_10092011CSK	–202.002	141
49	22042011CSK_19012012CSK	–974.933	272
50	22042011CSK_23032012CSK	133.606	336
51	22042011CSK_26082012CSK	165.877	492
52	08052011CSK_04022012CSK	269.593	272
53	08052011CSK_11092012CSK	304.813	492
54	24052011CSK_23032012CSK	–211.599	304
55	24052011CSK_10052012CSK	–187.615	352
56	09062011CSK_13092011CSK	–105.643	96
57	09062011CSK_16112011CSK	919.351	160
58	09062011CSK_15062012CSK	110.354	372
59	09062011CSK_09072012CSK	113.084	396
60	25062011CSK_11072011CSK	119.573	16
61	25062011CSK_03012012CSK	–86.413	192
62	25062011CSK_07032012CSK	60.482	256
63	25062011CSK_23062012CSK	–135.433	364
64	11072011CSK_28082011CSK	266.059	48
65	11072011CSK_07032012CSK	–590.857	240
66	11072011CSK_01102012CSK	56.313	448
67	28082011CSK_10092011CSK	300.423	13
68	28082011CSK_01102012CSK	297.073	400
69	10092011CSK_19012012CSK	104.566	131
70	10092011CSK_01102012CSK	–0.334317	387
71	13092011CSK_15102011CSK	–472.769	32
72	13092011CSK_09072012CSK	218.74	300
73	29092011CSK_15102011CSK	288.865	16
74	29092011CSK_20022012CSK	–819.955	144
75	15102011CSK_20022012CSK	–110.883	128
76	15102011CSK_09072012CSK	266.026	268
77	16112011CSK_15062012CSK	18.406	212
78	03012012CSK_23062012CSK	728.607	172
79	03012012CSK_25072012CSK	–86.681	204
80	03012012CSK_10082012CSK	–939.289	220
81	19012012CSK_26082012CSK	263.355	220
82	19012012CSK_01102012CSK	–107.889	256
83	04022012CSK_25072012CSK	322.286	172
84	04022012CSK_11092012CSK	352.751	220
85	20022012CSK_09072012CSK	376.928	140
86	07032012CSK_23062012CSK	–740.217	108
87	07032012CSK_01102012CSK	115.4	208
88	23032012CSK_10052012CSK	240.278	48
89	23032012CSK_26082012CSK	–117.014	156
90	08042012CSK_15062012CSK	–537.915	68
91	08042012CSK_09072012CSK	–510.744	92
92	08042012CSK_11092012CSK	296.571	156
93	10052012CSK_26082012CSK	–141.036	108
94	10052012CSK_01102012CSK	–178.145	144
95	15062012CSK_09072012CSK	272.147	24
96	23062012CSK_10082012CSK	–822.489	48
97	23062012CSK_01102012CSK	189.428	100
98	09072012CSK_11092012CSK	347.657	64
99	25072012CSK_10082012CSK	772.938	16
100	25072012CSK_11092012CSK	–286.986	48
101	10082012CSK_11092012CSK	–105.981	32
102	10082012CSK_01102012CSK	271.686	52
103	26082012CSK_01102012CSK	–371.231	36
104	11092012CSK_01102012CSK	377695	20

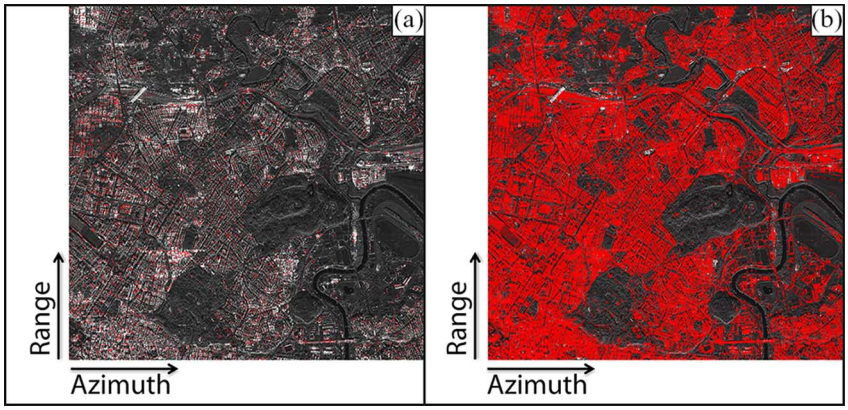

Fig. 4. Maps of coherent pixels, represented in red, related to (a) SPs and (b) TPs, superimposed on an amplitude SAR image (gray scale) of the city of Rome, Italy. The sets of pixels have been selected by imposing a threshold on the temporal coherence, (a) $\gamma \geq 0.9$ and (b) $0.4 < \gamma < 0.9$, respectively. Note also that radar coordinates are considered.

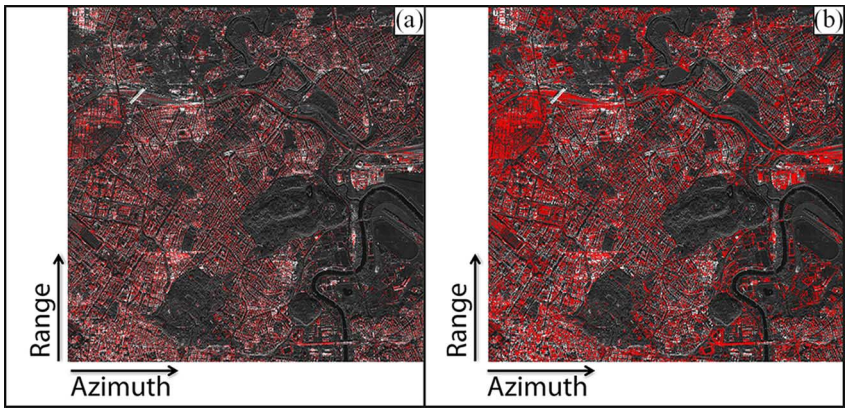

Fig. 5. (a) Map of coherent pixels retrieved at full resolution by applying the conventional SBAS-DInSAR approach, superimposed on an amplitude SAR image (radar coordinates) of the city of Rome. (b) Map of coherent pixels obtained after applying the C-NetP processing scheme. For both maps a temporal coherence threshold equal to 0.8 has been considered.

also contain phase contributions due to residual topography, atmospheric disturbances, and noise. Finally, the minimization operation in (6a) and (6b) [(7a)–(7c), in case $\mathrm{p} = 1$] is performed, thus requiring the generation of a CDT over the grid of the so-called target pixels, namely TPs, of the spatial azimuth/range domain, whose constrained edges are related to the set of SPs. TPs are efficiently identified by analyzing (again) the temporal coherence factor, but considering now a lower threshold, namely $\beta < \alpha$, i.e.,

$$\{TP\} = \{P \in A_Z \times R_G : \beta \leq \gamma(P) \leq \alpha\}. \qquad (10)$$

As a result of the solution of the optimization procedure in (6a) and (6b) [(7a)–(7c), in case $\mathrm{p} = 1$], the stack of M unwrapped phases at the TPs pixels $\psi(Q) = [\psi_1(Q), \psi_2(Q), \ldots, \psi_N(Q)]^T \; \forall Q \in \{TP\}$ is finally retrieved. They are subsequently inverted through the SBAS strategy [12], using the Singular Value Decomposition (SVD) method [55], to compute on propagated pixels the relevant displacement time series $\hat{\mathbf{d}}(Q) = [0, \hat{d}_1(Q), \hat{d}_2(Q), \ldots, \hat{d}_N(Q)]^T \; \forall Q \in \{TP\}$ as well as to provide an estimate of the residual topography $\hat{z}(Q)$. Finally, the map of the temporal coherence [31] is computed and the coherent target pixels are identified, the

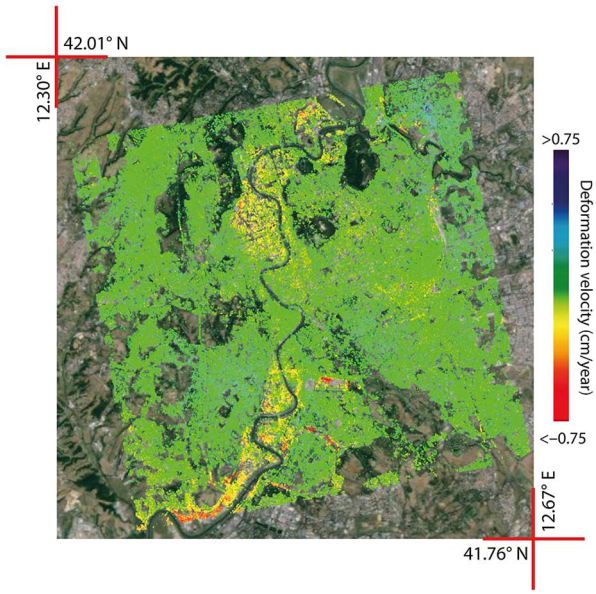

Fig. 6. Retrieved C-NetP mean deformation velocity map, superimposed on an optical image of the city of Rome, and relevant to the exploited 2010–2012 CSK data archive. An area of about 300 km^2 has been mapped for monitoring the deformation phenomena over the city of Rome.

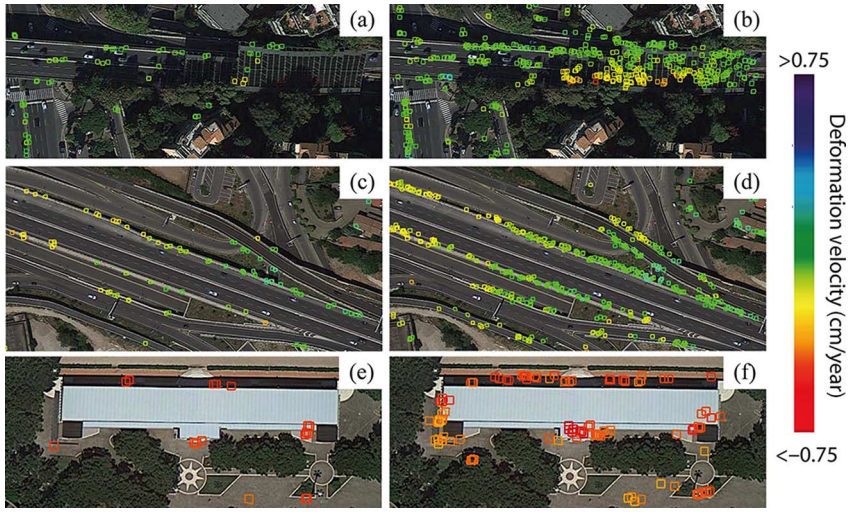

Fig. 7. Comparison between the zoomed views of full resolution conventional SBAS-DInSAR mean displacement maps (left side) and the ones achieved by using the proposed C-NetP processing strategy (right side), relevant to three selected areas.

atmospheric artefacts are estimated and filtered out [8], [12] from the retrieved displacement time series, thus obtaining the filtered $\hat{\mathbf{d}}_f(R) = [0, \hat{d}_1(R), \hat{d}_2(R), \ldots, \hat{d}_N(R)]^T \ \forall R \in TP \cup SP$ ones.

The block diagram of the developed C-NetP DInSAR processing scheme is shown in Fig. 3 for the readers' sake of convenience.

IV. Experimental Results

The overall performance of the proposed constrained C-NetP optimization scheme is here investigated through a series of experiments carried out on a sequence of full spatial resolution differential interferograms. As a case study, we selected the city of Rome (Italy), which is a heavily urbanized area, and for which a sequence of 40 SAR data frames collected over descending passes from July 7, 2010 to October 1, 2012 by the COSMO-SkyMed (CSK) radar constellation sensors (see Table I) was available. Based on the collected dataset, we first selected a group of 104 SB differential SAR interferograms characterized by perpendicular baseline values smaller than 400 m, which are listed in Table II. Satellite orbital information and a 3 arc-seconds shuttle radar topography mission (SRTM) [56] digital elevation model of the study area were also used to generate the sequence of single-look DInSAR interferograms, with a pixel size of about 3 m in the azimuth and range directions. As required by the preliminary stage of the C-NetP DInSAR scheme, the computed interferograms were analyzed through the "conventional" two-scale SBAS-DInSAR processing chain [13]. This has led, as a final outcome, to the generation of the displacement time series that represent the constraints of the constrained-network optimization problem to be subsequently implemented. Moreover, as a quality index of the retrieved displacement time series, for each pixel of the $A_Z \times R_G$ grid, the temporal coherence factor γ is124 computed.

To assess the performance of the C-NetP processing scheme to efficiently recover deformation time series in medium-to-low coherence areas (increasing the spatial density of DInSAR

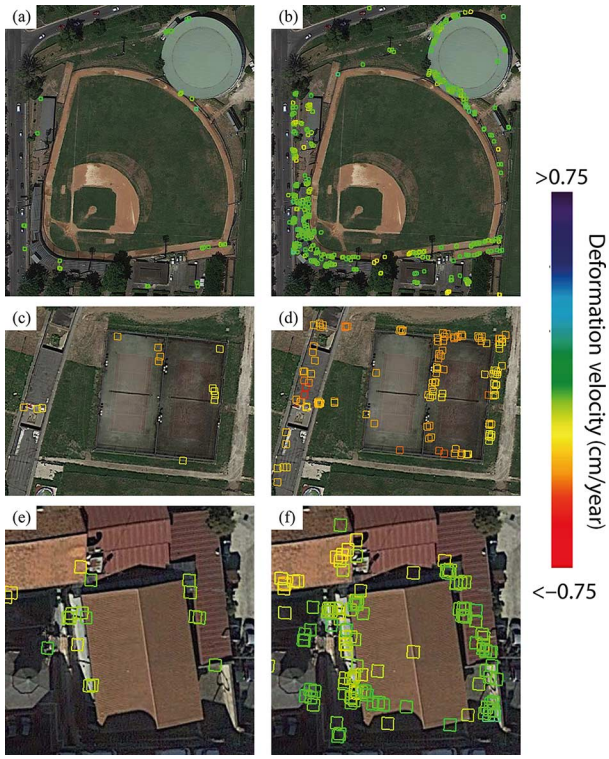

Fig. 8. Same as in Fig. 7, but now relevant to other three selected infrastructures.

measurements), we started by selecting the highly coherent SP pixels, which are less affected by noise and PhU errors. To do this, we considered a higher temporal coherence threshold ($\gamma = 0.9$), which is larger than the threshold (i.e., 0.8) applied to identify the coherent pixels in the SBAS-DInSAR analysis [23]. Therefore, a cluster of about 18 000 SPs have been identified, which are portrayed in Fig. 4(a), in correspondence to which displacement time series $\mathbf{d}(P) \ \forall P \in SP$, as well as estimates of the residual topography $z(P) \ \forall P \in SP$, are available. We remark that such a set of pixels does not represent the SBAS coherent points, but only a subset of them. From these SPs,

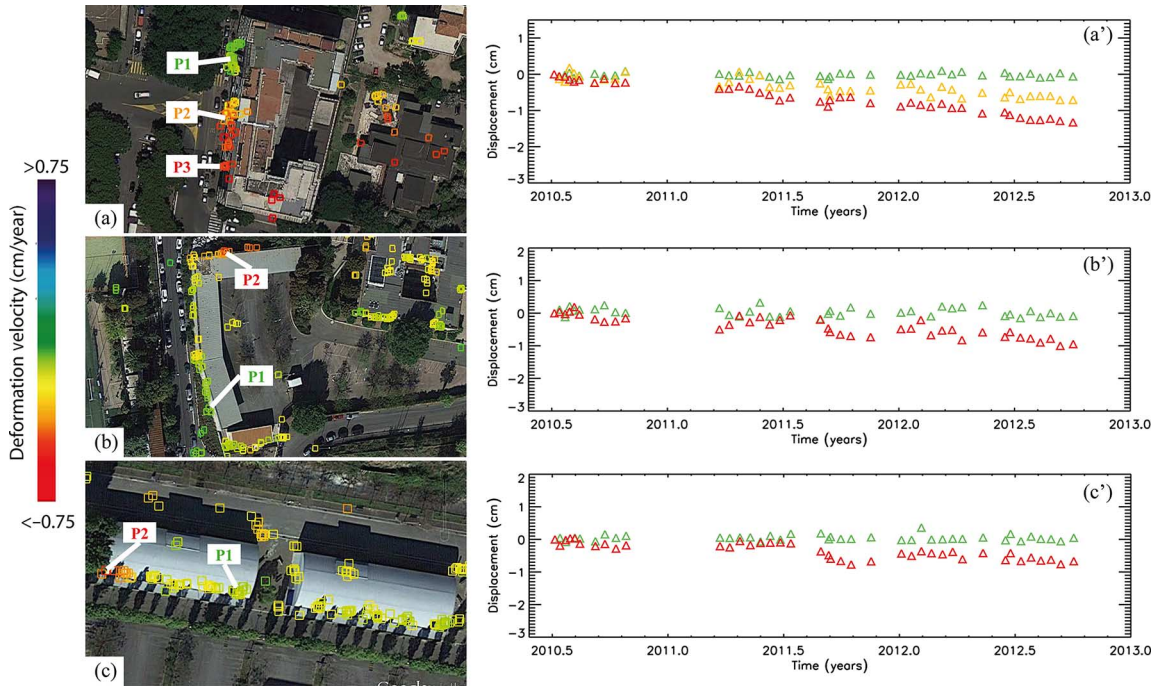

Fig. 9. (a)–(c) Zoomed view of the full resolution SBAS and C-NetP DInSAR velocity maps, superimposed on an optical image of the investigated areas corresponding to three infrastructures. The displacement time-series relevant to some points located on the three infrastructures are depicted in (a')–(c').

we generated a "primary network," forming a Delaunay triangulation in the $A_Z \times R_G$ spatial domain, which represents the backbone structure of the C-NetP scheme for further processing steps. More specifically, the L_1 PhU optimization problem in (7a)–(7c) was independently solved for each DInSAR interferogram. It corresponds to the "conventional" Minimum Cost Flow (MCF) PhU method in [42] and [43], and for which efficient solvers are currently, and freely, available in literature [45]. To this aim, a "secondary" network involving a group of low-to-moderate coherent SAR pixels [i.e., the targeted pixels (TPs)] was built in the $A_Z \times R_G$ spatial domain by computing a CDT, whose constrained arcs represent the edges of the "primary" network related to the high coherent SPs (i.e., the SPs). The TPs for the considered case study, which have been selected searching for SAR pixels with temporal coherence values γ ranging in the (0.4, 0.9) interval, are around 1.5 million and are shown in Fig. 4(b). As outcome of the application of the C-NetP processing scheme to TPs, we retrieved a cluster of about 470 000 SAR pixels, characterized, following the C-NetP processing, by a temporal coherence γ greater than 0.8. When compared with respect to conventional two-scale SBAS-DInSAR approach, our method has guaranteed an increase in the spatial density of coherent SAR pixels of about 250%, moving from the 136 000 (conventional SBAS processing) to 470 000 estimated "good" SAR pixels. For the sake of comparison, we portray in Fig. 5(a) and (b) the distribution of SAR coherent pixels as retrieved by applying the conventional as well as the C-NetP method, respectively. For each coherent target, an estimate of the topographic height inaccuracies of the used DEM was also obtained, which is taken into account for the correct estimation of displacement time series as well as for a correct geo-localization of obtained DInSAR products. The observed increase in the number of coherent points achieved by using the C-NetP technique is profitable to give a more detailed picture of ongoing deformation phenomena occurring over individual structures in the investigated areas, which can be either totally absent or characterized by a reduced number of independent measurement points in the conventional SBAS-DInSAR solution. The obtained DInSAR products have been geocoded and imported, for representation purposes, in Geographic Information System (GIS). For a correct pixel geolocalization procedure, both the residual topography and the SAR image Doppler centroids information [24], [28] have profitably been exploited. Fig. 6 shows a false color map of the detected mean deformation velocity of the city of Rome, which extends over an area of about $300\,\mathrm{km}^2$, where only points with high temporal coherence values (as said, we assumed a threshold $\gamma = 0.8$) are included. This comprehensive view of the velocity map highlights significantly larger deformation phenomena in the southern part of Rome along the Tevere River as compared to the northern sector of Rome. From previous works [57]–[60], performed with data collected by the first-generation SAR sensors ERS-1/2 and ENVISAT, it has already been examined that the predominant pattern of the displacement phenomena is due to the alluvial deposits along the Tevere river, which are responsible for a deformation with a rate of 1 cm/year or greater, and are associated with the compaction of more flexible soils in that zone. Moreover, in order to further investigate the effectiveness of the proposed C-NetP scheme, as compared with respect to the use of the conventional two-scale SBAS-DInSAR approach [13], we focused on a few selected areas over the city of Rome, highlighting specific infrastructures where several deformation signals are present. Accordingly, we display in Figs. 7 and 8 zoomed views of the mean displacement velocity maps as retrieved by the conventional (left side) and improved (right side) SBAS approaches,

respectively. In particular, in Fig. 7, three specific areas located on the northern side of Rome and their respective line-of-sight velocity maps are shown. The pictures highlight the deformation signals inferred by the C-NetP method corresponding to two street roads located in Via del Foro Italico [see Fig. 7(a) and (b)] and in Via dei Monti Tiburtini [see in Fig. 7(c) and (d)], respectively, as well as over one building [see Fig. 7(e) and (f)] located in the proximity of Via di Tor di Quinto. It is evident that the improvement in terms of density of detectable well-analyzed SAR pixels is drastic, allowing us to make it emerge deformation patterns that were hidden, or only in part visible, in the "conventional" SBAS velocity map. To further validate our analysis, we provide in Fig. 8 additional examples showing the distribution of detected coherent pixels related to one building located in Via Raiano [Fig. 8(a) and (b)], a baseball stadium located in the area of Via dei Campi Sportivi [Fig. 8(c) and (d)], and an isolated infrastructure in Viale dei Carabinieri a Cavallo [Fig. 8(e) and (f)]. Hence, from the above considerations and examples, it is clear that the application of the proposed C-NetP scheme has guaranteed a very significant improvement on the number of detectable radar targets w.r.t. the traditional full resolution two-scale SBAS method.

To complete our analysis and emphasize the robustness of the C-NetP approach in investigating the time evolution of deformation affecting targets on the ground, we finally selected three additional structures in the urbanized area of Rome, located nearby Viale Giustiniano imperatore [Fig. 9(a)], Via Mario Ageno [Fig. 9(b)] and Via Salvatore Pincherle [Fig. 9(c)], and we plotted their respective deformation time series corresponding to selected pixels laying on the imaged buildings, as shown in Fig. 9(a')–(c'). From the deformation time-series plots, it is noticeable that the subsidence pattern, for building in Fig. 9(a), is reaching up to 1 cm/year; similarly, buildings displayed in Fig. 9(b) and (c) have characterized by mostly linear trends in time reaching up cumulative displacements less than 2 cm in about the 2-year period of observation. These cases are important to further highlight how DInSAR-based approaches can be successfully used in urbanized areas to also monitor intra-buildings movements, which can cause severe stresses to load-bearing structures [28], [60].

V. Conclusion

In this paper, a solution to improve the retrieval capability of conventional two-scale SBAS-DInSAR approach, for the generation of deformation time series at full spatial resolution scale, has been proposed. The newly developed DInSAR scheme, referred to as Constrained-Network Propagation (C-NetP), is based on the analysis of a sequence of multitemporal SAR interferograms performed by solving a two-stage constrained-network optimization problem. The first step of the approach involves the knowledge of displacement time series in correspondence to a cluster of very coherent radar pixels, retrieved by applying the two-scale SBAS technique. The second step of the C-NetP method takes profit from the displacement values at such very coherent target location (SPs) to figure out which are the displacement time series at their neighboring locations by "propagating" the solution from highly to moderately coherent radar pixels (TPs). To preserve the high quality of DInSAR products corresponding to SPs, a constrained problem is casted. It relies on the computation of a CDT in the azimuth/range spatial domain, whose constrained edges connect one another previously identified SPs, and unconstrained edges are relevant to both SPs and TPs. Over these pixels, a constrained L_p minimization PhU procedure is properly applied, which is capable to retain the displacement time series at SPs location and to successfully propagate high-quality DInSAR measurements to their neighboring TPs. The reconstruction quality of displacement time series is checked, pixel-by-pixel, by computing the value of the temporal coherence, which is widely adopted for SBAS-DInSAR analyses.

The implemented C-NetP optimization scheme has primarily been developed as an extension of the two-scale full-resolution SBAS-DInSAR method; however, it can naturally be extended to work with other general-purpose SB- and PS-based DInSAR approaches. This can be done by simply modifying the way displacement time series are retrieved at SPs location (during the first stage of the algorithm), and at TPs ones (following the solution of the constrained optimization problem), without requiring any particular additional modifications on the adopted constrained-network optimization procedure used to "propagate" high-quality solutions from SPs to TPs. Furthermore, the method is able to easily incorporate in the optimization procedure displacement measurements coming from external sources, such as the ones inferred by GPS/leveling measurement campaigns. It is also worth remarking that the implemented constrained-network optimization relies on a very general constrained PhU strategy, giving potential users the possibility to adapt the algorithm to work with any of the existing PhU algorithms, with a limited number of adjustments. Accordingly, the specific characteristics of the proposed C-NetP method make it an effective and general tool for the estimation of displacement time series to be used in a wide spectrum of DInSAR-based applications, and for a very large set of SAR sensors and deformation scenarios. The achieved results demonstrate the C-NetP technique is competent for the mapping of displacement phenomena, especially in densely urbanized area. In this framework, it will not only play a key role for monitoring the individual physical process, which are responsible for the deformation phenomena, but will also act as a new advance operational tool in risk management as well as mitigation scenarios.

Acknowledgment

The authors would like to thank M. Bonano for her suggestions and comments, and S. Guarino, F. Parisi, and M. C. Rasulo for their technical support that has made possible the accomplishment of this work.

References

[1] R. Bürgmann, P. A. Rosen, and E. J. Fielding, "Synthetic aperture radar interferometry to measure Earth's surface topography and its deformation," *Annu. Rev. Earth Planet. Sci.*, vol. 28, pp. 169–209, May 2000.

[2] D. Massonnet and K. L. Feigl, "Radar interferometry and its application to changes in the Earth's surface," *Rev. Geophys.*, vol. 36, pp. 441–500, 1998.

[3] D. Massonnet *et al.*, "The displacement field of the Landers earthquake mapped by radar interferometry," *Nature*, vol. 364, pp. 138–142, Jul. 1993.

[4] D. Massonnet, P. Briole, and A. Arnaud, "Deflation of Mount Etna monitored by space borne radar interferometry," *Nature*, vol. 375, pp. 567–570, Jun. 1995.

[5] G. Peltzer and P. A. Rosen, "Surface displacement of the 17 May 1993 Eureka valley earthquake observed by SAR interferometry," *Science*, vol. 268, pp. 1333–1336, Jun. 1995.

[6] Y. Fialko, M. Simons, and D. Agnew, "The complete (3-D) surface displacement field in the epicentral area of the 1999 Mw 7.1 Hector Mine earthquake, California, from space geodetic observations," *Geophys. Res. Lett.*, vol. 28, pp. 3063–3066, Aug. 2001.

[7] E. Rignot, "Fast recession of a west Antarctic glacier," *Science*, vol. 281, pp. 549–551, 1998.

[8] A. Ferretti, C. Prati, and F. Rocca, "Permanent scatterers in SAR interferometry," *IEEE Trans. Geosci. Remote Sens.*, vol. 39, no. 1, pp. 8–20, Jan. 2001.

[9] C. Werner, U. Wegmüller, T. Strozzi, and A. Wiesmann, "Interferometric point target analysis for deformation mapping," in *Proc. IEEE Int. Geosci. Remote Sens. Symp. (IGARSS)*, Toulouse, France, Jul. 21–25, 2003, vol. 7, pp. 4362–4364.

[10] A. Hooper, H. Zebker, P. Segall, and B. M. Kampes, "A new method for measuring deformation on volcanoes and other natural terrains using InSAR persistent scatterers," *Geophys. Res. Lett.*, vol. 31, no. 23, p. L23 611, Dec. 2004, doi: 10.1029/2004GL021737.

[11] B. M. Kampes, *Radar Interferometry: Persistent Scatterer Technique*. New York, NY, USA: Springer, 2006.

[12] P. Berardino, G. Fornaro, R. Lanari, and E. Sansosti, "A new algorithm for surface deformation monitoring based on small baseline differential SAR interferograms," *IEEE Trans. Geosci. Remote Sens.*, vol. 40, no. 11, pp. 2375–2383, Nov. 2002.

[13] R. Lanari, O. Mora, M. Manunta, J. J. Mallorquì, P. Berardino, and E. Sansosti, "A small baseline approach for investigating deformation on full resolution differential SAR interferograms," *IEEE Trans. Geosci. Remote Sens.*, vol. 42, no. 7, pp. 1377–1386, Jul. 2004.

[14] S. Usai, "A least squares database approach for SAR interferometric data," *IEEE Trans. Geosci. Remote Sens.*, vol. 41, no. 4, pp. 753–760, Apr. 2003.

[15] O. Mora, J. J. Mallorquí, and A. Broquetas, "Linear and nonlinear terrain deformation maps from a reduced set of interferometric SAR images," *IEEE Trans. Geosci. Remote Sens.*, vol. 41, no. 10, pp. 2243–2253, Oct. 2003.

[16] M. Crosetto, B. Crippa, and E. Biescas, "Early detection and in-depth analysis of deformation phenomena by radar interferometry," *Eng. Geol.*, vol. 79, no. 1–2, pp. 81–91, Jun. 2005.

[17] H. A. Zebker and J. Villasenor, "Decorrelation in interferometric radar echoes," *IEEE Trans. Geosci. Remote Sens.*, vol. 30 no. 5, pp. 950–959, Sep. 1992.

[18] G. Franceschetti and R. Lanari, *Synthetic Aperture Radar Processing*. Boca Raton, FL, USA: CRC Press, Mar. 1999.

[19] F. Bovenga, R. Nutricato, A. Refice, and J. Wasowski, "Application of multi-temporal differential interferometry to slope instability detection in urban/peri-urban areas," *Eng. Geol.*, vol. 88, no. 3–4, pp. 218–239, Dec. 15, 2006.

[20] L. Cascini, S. Ferlisi, G. Fornaro, R. Lanari, D. Peduto, and G. Zeni, "Subsidence monitoring in Sarno urban area via multi-temporal DInSAR technique," *Int. J. Remote Sens.*, vol. 27, no. 8, pp. 1709–1716, 2006, doi: 10.1080/01431160500296024.

[21] S. Stramondo *et al.*, "Advanced DInSAR analysis on mining areas: La Union case study (Murcia, SE Spain)," *Eng. Geol.*, vol. 90, no. 3–4, pp. 148–159, Mar. 27, 2007.

[22] E. Sansosti, F. Casu, M. Manzo, and R. Lanari, "Space-borne radar interferometry techniques for the generation of deformation time series: An advanced tool for Earth's surface displacement analysis," *Geophys. Res. Lett.*, vol. 37, no. 20, pp. 1–9, Oct. 2010, doi: 10.1029/2010GL044379.

[23] R. Lanari *et al.*, "An overview of the small BAseline subset algorithm: A DInSAR technique for surface deformation analysis," *Pure Appl. Geophys.*, vol. 164, no. 4, pp. 637–661, Jan. 2007, doi: 10.1007/s00024-007-0192-9.

[24] M. Bonano, M. Manunta, M. Marsella, and R. Lanari, "Long-term ERS/ENVISAT deformation time-series generation at full spatial resolution via the extended SBAS technique," *Int. J. Remote Sens.*, vol. 33, no. 15, pp. 4756–4783, Feb. 2012, doi: 10.1080/01431161.2011.638340.

[25] M. Manzo, Y. Fialko, F. Casu, A. Pepe, and R. Lanari, "A quantitative assessment of DInSAR measurements of interseismic deformation: The Southern San Andreas fault case study," *Pure Appl. Geophys.*, vol. 169, no. 8, pp. 1463–1482, Aug. 2012.

[26] E. Trasatti *et al.*, "The 2004–2006 uplift episode at Campi Flegrei caldera (Italy): Constraints from SBAS-DInSAR ENVISAT data and Bayesian source inference," *Geophys. Res. Lett.*, vol. 35, no. 7, p. L07308, Apr. 2008.

[27] R. Lanari *et al.*, "Surface displacements associated with the L'Aquila 2009 Mw 6.3 earthquake (Central Italy): New evidence from SBAS-DInSAR time series analysis," *Geophys. Res. Lett.*, vol. 37, p. L20309, Oct. 2010.

[28] M. Bonano, M. Manunta, A. Pepe, L. Paglia, and R. Lanari, "From previous C-band to New X-band SAR systems: Assessment of the DInSAR mapping improvement for deformation time-series retrieval in urban areas," *IEEE Trans. Geosci. Remote Sens.*, vol. 51, no. 4, pp. 1973–1984, Apr. 2013.

[29] E. Sansosti *et al.*, "How second generation SAR systems are impacting the analysis of ground deformation," *Int. J. Appl. Earth Observ.*, vol. 28, no. 1, pp. 1–11, 2014, doi: 10.1016/j.jag.2013.10.007.

[30] A. Pepe, L. Euillades, M. Manunta, and R. Lanari, "New advances of the extended minimum cost flow phase unwrapping algorithm for SBAS-DInSAR analysis at full spatial resolution," *IEEE Trans. Geosci. Remote Sens.*, vol. 49, no. 10, pp. 4062–4079, Oct. 2011.

[31] A. Pepe and R. Lanari, "On the extension of the minimum cost flow algorithm for phase unwrapping of multi-temporal differential SAR interferograms," *IEEE Trans. Geosci. Remote Sens.*, vol. 44, no. 9, pp. 2374–2383, Sep. 2006.

[32] F. Covello *et al.*, "COSMO-SkyMed an existing opportunity for observing the Earth," *J. Geodyn.*, vol. 49, no. 3–4, pp. 171–180, Apr. 2010.

[33] U. Montanari, "Networks of constraints: Fundamental properties and applications to picture processing," *Inf. Sci.*, vol. 7, pp. 95–132, 1974.

[34] R. M. Goldstein, H. A. Zebker, and C. L. Werner, "Satellite radar interferometry: Two-dimensional phase unwrapping," *Radio Sci.*, vol. 23, pp. 713–720, 1988.

[35] D. C. Ghiglia and L. A. Romero, "Robust two-dimensional weighted and unweighted phase unwrapping that uses fast transforms and iterative methods," *J. Opt. Soc. Amer. A*, vol. 11, pp. 107–117, 1994.

[36] M. D. Pritt and J. S. Shipman, "Least-squares two-dimensional phase unwrapping using FFTs," *IEEE Trans. Geosci. Remote Sens.*, vol. 32, no. 3, pp. 706–708, May 1994.

[37] G. Fornaro, G. Franceschetti, and R. Lanari, "Interferometric SAR phase unwrapping using Green's formulation," *IEEE Trans. Geosci. Remote Sens.*, vol. 34, no. 3, pp. 720–727, May 1996.

[38] D. Kerr, G. H. Kaufmann, and G. E. Galizzi, "Unwrapping of interferometric phase-fringe maps by the discrete cosine transform," *Appl. Opt.*, vol. 35, no. 5, pp. 810–816, 1996.

[39] M. D. Pritt, "Phase unwrapping by means of multigrid techniques for interferometric SAR," *IEEE Trans. Geosci. Remote Sens.*, vol. 34, no. 3, pp. 728–738, May 1996.

[40] T. Flynn, "Two-dimensional phase unwrapping with minimum weighted discontinuity," *J. Opt. Soc. Amer. A*, vol. 14, no. 10, pp. 2692–2701, 1997.

[41] G. Fornaro, G. Franceschetti, R. Lanari, D. Rossi, and M. Tesauro, "Interferometric SAR phase unwrapping using the finite element method," *IEE Proc. Radar Sonar Navigat.*, vol. 144, no. 5, pp. 266–274, Oct. 1997.

[42] M. Costantini, "A novel phase unwrapping method based on network programming," *IEEE Trans. Geosci. Remote Sens.*, vol. 36, no. 3, pp. 813–821, May 1998.

[43] M. Costantini and P. A. Rosen, "A generalized phase unwrapping approach for sparse data," in *Proc. Geosci. Remote Sens. Symp. (IGARSS)*, Hamburg, Germany, Jun. 1999, pp. 267–269.

[44] B. Delaunay, "Sur la sphère vide. A la mémoire de Georges Voronoï," *Bulletin de l'Académie des Sciences de l'URSS, Classe des Sciences Mathématiques et Naturelles*, no. 6, pp. 793–800, 1934.

[45] D. P. Bertsekas and P. Tseng, "Relaxation methods for minimum cost ordinary and generalized network flow problems," *Oper. Res.*, vol. 36, no. 1, pp. 93–114, Jan./Feb. 1988.

[46] L. Paul Chew, "Constrained Delaunay triangulations," *Algorithmica*, vol. 4, pp. 97–108, 1989.

[47] M. Kallmann, H. Bieri, and D. Thalmann, "Fully dynamic constrained Delaunay triangulations," in *Geometric Modeling for Scientific Visualization*, Part IV. New York, NY, USA: Springer, 2004, pp. 241–257.

[48] M. Qi, T. T. Cao, and T. S. Tan, "Computing 2D constrained Delaunay triangulation using the GP," in *Proc. ACM SIGGRAPH Symp. Interactive 3D Graph. Games*, Mar. 2012, pp. 39–46.

[49] R. K. Ahuja, T. I. Magnanti, and J. B. Orlin, *Network flows: Theory, algorithms, and applications*. Englewood ClitTs, NJ, USA: Prentice Hall, Feb. 1993.
[50] K. Mehlhorn and M. Ziegelmann, "CNOP—A package for constrained network optimization," in *Proc. Algorithm Eng. Exp. (ALENEX'01)*, LNCS, 2001, vol. 2153, pp. 17–31.
[51] A. Hooper and H. Zebker, "Phase unwrapping in three dimensions with applications to InSAR time series," *J. Opt. Soc. Amer. A, Opt. Image Sci.*, vol. 24, no. 9, pp. 2737–3747, Aug. 2007.
[52] M. Costantini, S. Falco, F. Malvarosa, F. Minati, F. Trillo, and F. Vecchioli, "A general formulation for robust integration of finite differences and phase unwrapping on sparse multidimensional domains," in *Proc. Fringe*, Frascati, Italy, Dec. 2009.
[53] G. Fornaro, A. Pauciullo, and D. Reale, "A null-space method for the phase unwrapping of multitemporal SAR interferometric stacks," *IEEE Trans. Geosci. Remote Sens.*, vol. 49, no. 6, Part 2, pp. 2323–2334, Jun. 2011, doi: 10.1109/TGRS.2010.2102767.
[54] F. Rossi, P. van Beek, and T. Walsh, *Handbook of Constraint Programming*. Amsterdam, The Netherlands: Elsevier, 2006.
[55] G. Strang, *Linear Algebra and Its Appications*. Orlando, FL, USA: Harcourt Brace Jovanovich, 1988.
[56] P. A. Rosen, S. Hensley, E. Gurrola, F. Rogez, S. Chan, and J. Martin, "SRTM C-and topographic data: Quality assessment and calibration activities," in *Proc. Int. Geosci. Remote Sens. Symp. (IGARSS)*, 2001, pp. 739–741.
[57] M. Manunta, M. Marsella, G. Zeni, M. Sciotti, S. Atzori, and R. Lanari, "Two-scale surface deformation analysis using the SBAS-DInSAR technique: A case study of the city of Rome, Italy," *Int. J. Remote Sens.*, vol. 296, pp. 1665–1684, 2008.
[58] S. Stramondo *et al.*, "Subsidence induced by urbanisation in the city of Rome detected by advanced InSAR technique and geotechnical investigations," *Remote Sens. Environ.*, vol. 112, no. 6, pp. 3160–3172, 2008.
[59] G. Zeni *et al.*, "Long term deformation analysis of historical buildings through the advanced SBAS-DInSAR technique: The case study of the city of Roma Italy," *J. Geophys. Eng.*, vol. 8, pp. S1–S12, 2001, doi: 101088/1742-2132/8/3/S01.
[60] S. Arangio, F. Calò, M. Di Mauro, M. Bonano, M. Marsella, and M. Manunta, "An application of the SBAS-DInSAR technique for the assessment of structural damage in the city of Rome," *Struct. Infrastruct. Eng. Maintenance Manage. Life Cycle Des. Perform.*, vol. 10, pp. 1469–1483, 2014.

Chandrakanta Ojha received the M.Sc. degree in physics from the University of Delhi, New Delhi, India, in 2008, the M.Tech. degree in natural resources engineering from the Indian Institute of Technology (IIT), Bombay, India, in 2011, and the Ph.D. degree in civil and environmental engineering from the University of Rome "Sapienza" Rome, Italy, in 2015.

Since 2012, he has been a Research Fellow with the Istituto per il Rilevamento Elettromagnetico dell'Ambiente (IREA), a Research Institute of the Italian National Research Council (CNR), Naples, Italy. His research interests include synthetic aperture radar (SAR) data processing, multitemporal differential SAR interferometry, parallel computing, and compressive sensing.

Michele Manunta was born in Cagliari, Italy, in 1975. He received the Laurea degree in electronic engineering in 2001, and the Ph.D. degree in informatics and electronic engineering from the University of Cagliari, Cagliari, Italy, in 2009.

Since 2002, he has been with the Istituto per il Rilevamento Elettromagnetico dell'Ambiente (IREA), an Institute of the Italian National Research Council (CNR), Naples, Italy, where he currently holds a Researcher Position. He was a Visiting Scientist at the Institut Cartografic de Catalunya, Barcelona, Spain, in 2004, and the Rosenstiel School of Marine and Atmospheric Science, University of Miami, Coral Gables, FL, USA, in 2006. He has been collaborating in various national and international initiatives for the exploitation of satellite technologies, and in particular of SAR techniques. His research interests include high-resolution SAR, DInSAR data processing and application, and cloud and GRID computing exploitation for SAR interferometry applications.

Riccardo Lanari (M'91–SM'01–F'13) received the degree in electronic engineering (*summa cum laude*) from the University of Napoli, Federico II, Naples, Italy, in 1989.

In 1989, following a short experience at ITALTEL SISTEMI SPA, he joined IRECE and after Istituto per il Rilevamento Elettromagnetico dell'Ambiente (IREA), a Research Institute of the Italian National Research Council (CNR), Naples, Italy, where, since November 2011, he has been the Institute Director. He has lectured in several national and foreign universities and research centers. He was an Adjunct Professor of Electrical Communication with the l'Università del Sannio, Benevento, Italy, from 2000 to 2003, and from 2000 to 2008, he was the Lecturer of the synthetic aperture radar (SAR) module course of the International Master in Airbone Photogrammetry and Remote Sensing offered by the Institute of Geomatics, Barcelona, Spain. He was a Visiting Scientist at different foreign research institutes, including the Institute of Space and Astronautical Science, Sagamihara, Japan, in 1993; German Aerospace Research Establishment (DLR), Cologne, Germany, in 1991 and 1994; and Jet Propulsion Laboratory, Pasadena, CA, USA, in 1997, 2004, and 2008. Moreover, he acts as a Reviewer of several peer-reviewed international journals. His research interests include the SAR data processing field as well as in SAR interferometry techniques; on this topic, he is the holder of two patents, and he has authored or coauthored 80 international journal papers and the book *Synthetic Aperture Radar Processing* (1999, CRC Press).

Mr. Lanari is a Distinguished Speaker of the Geoscience and Remote Sensing Society of the IEEE, and he has served as the Chairman and as a Technical Program Committee Member at several international conferences. He was the recipient of the NASA recognition and a Group Award for the technical developments related to the Shuttle Radar Topography Mission

Antonio Pepe (M'12) received the Laurea degree in electronic engineering and the Ph.D. degree in electronic and telecommunication engineering from the University of Napoli Federico II, Naples, Italy, in 2000 and 2007, respectively.

After graduation, following a short experience with Wind Telecommunication S.p.A., Rome, Italy, he joined the Istituto per il Rilevamento Elettromagnetico dell'Ambiente (IREA), Italian National Research Council (CNR), Naples, Italy, in 2001, where he currently holds a permanent position of Researcher. He was a Visiting Scientist at the University of Texas at Austin, Austin, TX, USA, in 2005, at the Jet Propulsion Laboratory (JPL), Caltech, Pasadena, CA, USA, in 2009, and at the East China Normal University (ECNU), Shanghai, China, in 2014. He acts as a Reviewer of several peer reviewed international journals. Since 2012, he has also been an Adjunct Professor of Signal Theory at the Università della Basilicata, Potenza, Italy. More recently, he has developed research activities for the generation of DInSAR products through new generation SAR instruments, for the generation of mixed ScanSAR-Stripmap DInSAR analyses, and for the integration of SAR and optical imagery. His research interests include the development of advanced DInSAR algorithms aimed at monitoring surface deformation phenomena induced by subsidence, volcano activities, and earthquakes, with a particular interest toward the phase unwrapping problems.

Dr. Pepe is a member of the Editorial Board of the Advances in Geology and *Asian Journal of Geoscience* journals, Hindawi Publishing Corporation. He was the recipient of the 2014 Best Reviewer mention of the IEEE GEOSCIENCE AND REMOTE SENSING LETTERS.